Structural Consequences of Ammonia Binding to the Manganese Center of the Photosynthetic Oxygen-Evolving Complex: An X-ray Absorption Spectroscopy Study of Isotropic and Oriented Photosystem II Particles†

Holger Dau,*,‡,§,∥ Joy C. Andrews,‡,§ Theo A. Roelofs,‡,§ Matthew J. Latimer,‡,§ Wenchuan Liang,‡,§ Vittal K. Yachandra,*,§ Kenneth Sauer,*,‡,§ and Melvin P. Klein*,§

Structural Biology Division, Lawrence Berkeley Laboratory, and Department of Chemistry, University of California, Berkeley, California 94720

Received June 28, 1994; Revised Manuscript Received February 6, 1995®

ABSTRACT: The structure and orientation of the manganese complex in NH_3-treated photosystem II (PS II) membrane particles of spinach are being studied by X-ray absorption spectroscopy. On the basis of earlier work by our group, a structure for the tetranuclear manganese complex of PS II, which consists of two di-μ-oxo-bridged binuclear Mn units linked by a mono-μ-oxo group, has been proposed [Yachandra, V. K., et al. (1993) *Science 260*, 675−679]. The extended X-ray absorption fine structure (EXAFS) of the complex modified by NH_3 binding in the S_2-state is suggestive of an increase in the Mn−Mn distance of one of these units from 2.72 ± 0.02 to 2.87 ± 0.02 Å, whereas the Mn−Mn distance of the second unit seems to be unaffected by NH_3 treatment. The elongation of one binuclear center could result from the replacement of one bridging μ-oxo by an amido group. The lengthening of one Mn−Mn distance means that, by NH_3 treatment, the distance degeneracy of the 2.7 Å Mn−Mn EXAFS interaction is removed. Consequently, the orientation of individual binuclear units with respect to the membrane normal becomes resolvable by EXAFS spectroscopy of partially oriented PS II membrane particles. The angle between the normal of the PS II-containing membrane and the Mn−Mn vector is determined to be 67° ± 3° for the 2.87 Å distance and 55° ± 4° for the 2.72 Å distance. Only small effects on position, shape, and orientation dependence of Mn K-edge spectra result from NH_3 treatment, indicating that the Mn oxidation state, the symmetry of the Mn ligand environment, and the orientation of the complex remain essentially unaffected in the annealed NH_3 S_2-state. Therefore, it seems likely that the angles determined for the ammonia-modified manganese complex are similar to the respective angles of the untreated complex. The structure of the manganese complex and its orientation in the membrane are discussed.

The molecular structure of the intermediates as well as the reaction mechanism involved in the utilization of water as an electron donor for the light-driven electron transfer reactions of photosynthesis are still only inadequately understood. For recent reviews on photosynthetic water oxidation, see Rutherford et al. (1992) and Debus (1992). The water oxidase is associated with photosystem II (PS II),[1] a membrane-spanning multiprotein complex of about 500 kDa. Following the absorption of a photon by the PS II antenna pigments, a primary charge separation reaction is initiated, which results in the reduction of a special pheophytin and the oxidation of P_{680}. The primary electron donor P_{680} is re-reduced by a tyrosine residue, and the oxidized tyrosine delivers one oxidizing equivalent to an entity called the oxygen-evolving complex (OEC), which is defined by its function (the accumulation of oxidizing equivalents, water oxidation, and release of molecular oxygen) rather than by its physical identity. Driven by the one-electron oxidation that results from the absorption of a single photon, the OEC advances from the S_n-state to the S_{n+1}-state, where the subscripts give the number of oxidizing equivalents accumulated by the OEC. The most oxidized state of the OEC, the S_4-state, spontaneously relaxes to the S_0-state concurrently with the release of dioxygen (Kok et al., 1970), which stems from two water molecules. The S_0- and S_1-states are dark-stable; upon prolonged dark adaptation, the S_1-state is predominant.

The catalytic center of the OEC is widely believed to contain a tetranuclear, mixed-valence manganese complex [reviewed in Debus (1992)]. Two of the sources for structural information on the PS II Mn complex and its protein environment have been metal-specific spectroscopic techniques: electron paramagnetic resonance (EPR) and X-ray absorption spectroscopy (XAS) (Brudvig & Beck 1992; Sauer et al., 1992; Klein et al., 1993; Wieghardt, 1994).

† This research was supported by the Director, Office of Basic Energy Sciences, Division of Energy Biosciences of the U.S. Department of Energy, under Contract No. DE-AC03-76SF00098, and by a grant from the National Science Foundation (DMB91-04104). H.D. was supported by the Deutsche Forschungsgemeinschaft (SFB 305, Projekt B1) and by a Feodor Lynen Fellowship of the Alexander von Humboldt-Stiftung. Support from a NATO Collaborative Research Grant (to V.K.Y. and H.D.) is acknowledged.

* Authors to whom correspondence should be addressed.

‡ Department of Chemistry.

§ Structural Biology Division.

∥ Present address: FB Biologie/Botanik, Philipps-Universität Marburg, Lahnberge, D-35032 Marburg, Germany.

® Abstract published in *Advance ACS Abstracts,* April 1, 1995.

[1] Abbreviations: Chl, chlorophyll; cyt, cytochrome; EPR, electron paramagnetic resonance; ESEEM, electron spin echo envelope modulation; EXAFS, extended X-ray absorption fine structure; HEPES, *N*-(2-hydroxyethyl)piperazine-*N*′-2-ethanesulfonic acid; MES, 4-morpholinoethanesulfonic acid; OEC, oxygen-evolving complex; PPBQ, phenyl-*p*-benzoquinone; PS II, photosystem II; XAS, X-ray absorption spectroscopy.

0006-2960/95/0434-5274$09.00/0

X-ray absorption spectroscopy on PS II preparations involves measurements of the fluorescence-detected X-ray absorption spectra with excitation energies at and above the Mn K-edge and detection of the Mn fluorescence. Due to the selective excitation and detection of the Mn X-ray fluorescence, this technique allows the investigation of the Mn complex without interference from pigment molecules, the lipid and protein matrix, or other metals such as Ca, Mg, Cu, or Fe that are present in oxygen-evolving PS II preparations. The Mn K-edge and pre-edge spectra provide information about the oxidation states and the site symmetry of the Mn complex. The extended X-ray absorption fine structure (EXAFS) results from interactions between the absorbing Mn atom and the backscattering from ligand and neighboring atoms of Mn. EXAFS spectra provide information about the numbers, types, and distances of the backscattering atoms from the absorbing Mn atoms [reviewed in Sauer et al. (1992)]; data evaluation techniques to extract this structural information from EXAFS spectra are available (Teo, 1986; Koningsberger & Prins, 1988). It is generally agreed that the 2.7 Å absorber−backscatterer interaction found by EXAFS spectroscopy originates from pairs of Mn atoms linked by at least two single-atom bridges and that the single-atom bridges could be μ-oxo bridges (Kirby et al., 1981; Yachandra et al., 1986; George et al., 1989; Penner-Hahn et al., 1990; MacLachlan et al., 1992). The 3.3 Å distance found by EXAFS spectroscopy is assigned to Mn−Mn and/or Mn−C and/or Mn−Ca EXAFS interactions (Guiles et al., 1987; George et al., 1989; Penner-Hahn et al., 1990; DeRose, 1990; Yachandra et al., 1992, 1993).

As a structural model for the manganese complex, we have proposed two di-μ-oxo-bridged Mn binuclear structures in a cis configuration with a distance of 3.3 Å between the two closest Mn atoms of adjacent binuclear structures, which are linked by a mono-μ-oxo group (Yachandra et al., 1993). This model is in good agreement with the results of EXAFS and EPR studies. However, other chemically feasible structures exist that do not contradict present EXAFS and EPR results (DeRose et al., 1994). Only as more structural information becomes available will an unambiguous structural model eventually emerge.

A promising new approach to obtain more detailed structural information is EXAFS spectroscopy on oriented PS II (George et al., 1989; Yachandra et al., 1993; Mukerji et al., 1994). By collecting EXAFS data sets for several angles between the electric field vector (of the exciting X-ray beam) and the sample, information about the orientation of absorber−backscatterer distances becomes accessible. One may call this technique X-ray absorption linear dichroism spectroscopy. Partial orientation of the PS II protein complex is achievable by a paint and dry procedure applied to thylakoid membranes (Hales & Das Gupta, 1981) or to PS II membrane particles (Rutherford, 1985). The use of this procedure results in a preferred orientation of the membrane plane parallel to the underlying surface. In principle, EXAFS measurements on the partially oriented samples allow the determination of the angle between the absorber−backscatterer vector and the membrane normal. However, if several internuclear distances are identical, only an average angle can be determined (George et al., 1989, 1993). In studies of oriented native PS II (Mukerji et al., 1994), it was not possible to distinguish between the two Mn−Mn 2.7 Å vectors. However, in this study of ammonia-modified PS II preparations, the distance degeneracy of the 2.7 Å vectors is removed, and the average angle limitation of the dichroism technique is overcome.

NH_3 is an analog of substrate H_2O and also is an inhibitor of water oxidation. Hind and Whittingham (1963) studied the inhibitory effect of NH_4Cl on ferricyanide reduction by illuminated chloroplasts as a function of pH. They concluded that the inhibition is caused by the unprotonated base ammonia. Izawa et al. (1969) demonstrated that the inhibition by NH_3 occurs by blocking water oxidation. Velthuys (1975) provided kinetic resolution to the study of NH_3 inhibition of oxygen evolution by measuring the effects of ammonia on the flash-induced luminescence of chloroplasts. This study suggested the presence of ammonia binding sites at the S_2 and S_3 states of the Kok S-state cycle. Sandusky and Yocum (1984, 1986) described two independent sites of ammonia inhibition. The type I site (SY I) shows inhibition by the class of amines that are competitive with Cl^-. The second ammonia inhibition site (SY II) was accessible only to ammonia, and the ammonia binding was not competitive with respect to Cl^-. Sandusky and Yocum proposed the second binding site to be normally occupied by the substrate water. These findings spurred many EPR studies on ammonia binding, reviewed extensively by Rutherford et al. (1992), Debus (1992), and Brudvig and Beck (1992). The binding to the second ammonia site, which does not occur in the S_0- or S_1-state of the OEC or at low temperature, modifies the EPR multiline signal of the Mn complex in the S_2-state (Beck et al., 1986). This modified multiline EPR was interpreted as ligation of NH_3 to Mn. Britt et al. (1989) presented electron spin echo envelope modulation (ESEEM) data with evidence in favor of an amido (NH_2) bridge between metal ions.

Because it is proposed that NH_3 inhibits O_2 evolution by binding at the site of water binding, it is important that one understands the structural effects such inhibition produces. As reported in this article, EXAFS measurements indicate that binding of NH_3 in the S_2-state to the second binding site (SY II) causes an increase in one 2.7 Å Mn−Mn distance by 0.15 Å. Thus, in the state that is characterized by the ammonia-modified multiline signal, the distance degeneracy of 2.7 Å Mn−Mn binuclear units is removed, and by EXAFS measurements, individual binuclear units become resolvable. Measurements on oriented NH_3-treated PS II membrane particles demonstrate that X-ray absorption linear dichroism spectroscopy is feasible for this preparation, and angles for the orientation of individual Mn−Mn vectors are obtainable. The Mn K-edge spectra of oriented and nonoriented samples provide evidence that NH_3 treatment does not result in major changes in the symmetry of the Mn ligand environment or in the orientation of the complex.

MATERIALS AND METHODS

Preparation of PS II Membranes for X-ray Absorption Measurements. Preparation of O_2-evolving PS II membrane particles was accomplished by a modification of the Triton X-100 procedure of Berthold et al. (1981). All steps of the preparation procedure were performed under dim green light at about 4 °C. Leaves of fresh market spinach were washed in ice water, destemmed, and ground in a Waring blender for 10 s in a medium containing 20 mM HEPES (pH 7.5)/0.4 M NaCl/1 mM EDTA/5 mM ascorbic acid/2 mg mL^{-1}

bovine serum albumin. The homogenate was filtered through cheesecloth twice (2 and 18 layers, respectively) and centrifuged for 6 min at 5000*g*. The chloroplast pellet was resuspended in 25 mM HEPES (pH 7.5)/150 mM NaCl/8 mM $MgCl_2$ and spun for 10 min at 5000*g*. The resulting pellet, consisting of intact thylakoid membranes, was suspended in a small amount of resuspension buffer (R buffer: 50 mM MES, (pH 6.0)/15 mM NaCl/10 mM $MgCl_2$). This thylakoid suspension was diluted with R buffer and a 25% Triton X-100 solution to give a final Triton-to-Chl ratio (w/w) of 25:1, with a final concentration of 2 mg of Chl mL^{-1}. Triton incubation was carried out in the dark by very gentle stirring for 25 min. After incubation, the suspension was spun for 20 min at 38000*g*. The pellet was resuspended in R buffer and centrifuged for 2 min at 500*g* to remove cell debris and starch; the resulting pellet was discarded. The supernatant, which contained the PS II membrane fraction, was spun for 10 min at 38000*g*.

For control samples, the PS II membrane pellet of the previous step was washed first in R buffer and then in a cryoprotectant-containing buffer (50 mM MES (pH 6.0)/15 mM NaCl/5 mM $MgCl_2$/5 mM $CaCl_2$/400 mM sucrose), each time followed by centrifugation for 30 min at 38000*g*. After these washing steps, O_2 evolution rates of 450−650 μmol of O_2/(mg of Chl·h) were assayed. The pellet of the last centrifugation step was transferred to the X-ray sample holders and frozen in liquid nitrogen. The X-ray sample holders consisted of a lucite frame (inner dimensions 22 × 4 × 2 mm) and a back wall of thin, metal-free Mylar tape.

For NH_3 treatment, the PS II membrane pellet was washed first in 40 mM HEPES (pH 7.5)/50 mM NaCl/0.4 M sucrose and then in 40 mM HEPES (pH 7.5)/5 mM NaCl/0.4 M sucrose, each time followed by centrifugation for 15 min at 38000*g*. The PS II electron acceptor PPBQ (30 mM in ethanol) was added to the pellet of the last centrifugation step, resulting in a final PPBQ concentration of about 0.8 mM and a final ethanol content of about 2% (v/v); NH_4Cl solution (2 M, adjusted with NaOH to pH 7.5) was added to give a final NH_4Cl concentration of approximately 100 mM (Kim et al., 1992). Finally, the suspension (about 25 mg of Chl/mL) was transferred to the X-ray sample holders described earlier and frozen in liquid nitrogen.

The X-ray samples, prepared as described earlier, were predominantly in the S_1-state because they were fully dark-adapted. To establish the S_2-state, the X-ray samples were illuminated for 8 min at 195 K (Brudvig et al., 1983). To create the state that is associated with the ammonia-modified EPR multiline signal (Beck et al., 1986), the ammonia-treated samples were illuminated at 195 K and annealed by exposure for 60 s to a stream of nitrogen gas at about 4 °C (Kim et al., 1992); after this annealing procedure, the X-ray samples were quickly frozen in liquid nitrogen.

Preparation of Oriented PS II Membranes. Mylar tape was glued onto a supporting lucite frame (26 × 5 mm outer dimensions). The PS II membrane suspension was painted with a fine brush onto the glue-free side of the Mylar tape and dried for 20 min under a gentle stream of nitrogen gas (in the dark at 4 °C). Upon drying, the membrane sheets settle onto the Mylar tape with a preferred orientation of the membrane plane parallel to the tape plane (concerning the degree of orientation, see Results). After drying for 20 min, another layer of the PS II membrane suspension was painted on top of the first layer. The painting and drying procedure was done three times in order to triple the amount of PS II per X-ray sample. Finally, the samples were frozen by immersion in liquid nitrogen.

EPR Spectra. Low-temperature X-band EPR spectra were recorded using a Varian E109 EPR spectrometer equipped with an E-102 microwave bridge, an Air Products liquid helium cryostat, and a goniometer for rotating oriented samples with respect to the magnetic field. The temperature of the sample was monitored using a gold−chromel thermocouple junction. The structural integrity (absence of free manganese) and the functional states (S_1, S_2, annealed NH_3 S_2) of all X-ray samples were routinely verified by means of EPR measurements, before and after exposure to X-rays. Illumination of NH_3-treated PS II samples at 195 K generated a multiline EPR spectrum with a characteristic average hyperfine line spacing of about 88 G. As first reported by Beck et al. (1986), annealing of the NH_3-treated samples as described earlier induced a modified multiline EPR signal characterized by a larger number of hyperfine lines, with an average spacing of about 67 G. The modified multiline EPR spectrum was used as a criterion for evaluating the quality of the ammonia-inhibited PS II samples.

X-ray Absorption Measurements. The X-ray absorption spectra were recorded at the Stanford Synchrotron Radiation Laboratory (Stanford, CA) on wiggler beam lines IV-2 (for EXAFS spectra) and VII-3 (for K-edge spectra), using Si-⟨220⟩ and Si⟨111⟩ double-crystal monochromators, respectively. Some of the spectra were recorded at the National Synchrotron Light Source (Upton, NY) on beam line X9A.

X-ray spectra were collected using an energy-resolving 13-element Ge solid-state detector (Canberra Instruments) (Cramer et al., 1988) and a liquid helium flow cryostat (Oxford Instruments CF 1204) operated at 10 ± 1 K. Fluorescence excitation spectra were recorded by detection of the Mn fluorescence with X-ray excitation energies ranging from 6500 to 6600 eV or 7100 eV for edge or EXAFS spectra, respectively. By adjustment of the slits, the beam dimensions were set to be approximately equal to the inner dimensions of the sample frame, i.e., 22 × 4 mm. For EXAFS spectra, 15−30 energy scans of about 25 min each were recorded and averaged. Energy calibration in the X-ray experiment was maintained by simultaneously monitoring the narrow pre-edge feature of a $KMnO_4$ standard (Goodin et al., 1979). For edge spectra (Si⟨111⟩ crystals), the full width at half-maximum of this pre-edge feature was 1.8 ± 0.2 eV. The recorded fluorescence excitation spectra are essentially identical to the respective X-ray absorption spectra. Therefore, in the following the excitation spectra are referred to as absorption spectra.

EXAFS Data Analysis. All data analysis was done on a VAX 4000-300. The amplitude in the region below the onset of the Mn K-edge was set to zero by subtraction of a linear fit to the spectrum below the edge. Postedge spectra were divided by the free atom absorption of Mn and normalized to a unit edge jump determined by the extrapolation of a quadratic fit of the postedge absorption to the energy of the first major absorption peak. A quadratic fit to the postedge spectrum was subtracted from the postedge data.

The absorption versus X-ray energy data were converted into *k*-space data by transforming the energy scale into a

wavenumber scale according to

$$k = (2\pi/h)[2m_e(E - E_0)]^{1/2} \quad (1)$$

where m_e is the electron mass, E is the X-ray energy, and E_0 is the edge energy. We used an E_0 of 6563.0 eV (the approximate position of the edge peak). Then the absorption values were multiplied by k^3. The k^3-weighted data were fit to low-order polynomial functions (cubic splines) and corrected for this smooth background by subtracting the fit result.

The Fourier transforms of the k^3 data were calculated using a k range of 3.5−11.5 Å^{-1} for the isotropic samples and 3.5−11.9 Å^{-1} for the oriented samples. Individual peaks of the Fourier-transformed k^3-weighted data were isolated by applying a Hamming window function to the first and last 15% of the data, leaving the middle 70% untouched. These individual peaks were back-transformed, yielding the Fourier-isolated k-space data. The Fourier-isolated data were subjected to curve fitting. Further details of the analysis of EXAFS data have been described previously (Goodin et al., 1979; Kirby et al., 1981; Guiles et al., 1988; DeRose, 1990).

Detailed structural information regarding the number of ligands and distances is obtained by fitting the Fourier-isolated k-space data to its known functional form (Teo, 1986). The following functions were used for curve fitting of the Fourier-isolated data:

$$k^3\chi(k) = k^3\sum_i \frac{N_i|f_i(\theta,k)|}{kR_i^2}\exp(-2\sigma_i^2k^2)\sin[2kR_i + \alpha_i(k)] \quad (2)$$

where $k^3\chi(k)$ is the experimentally determined k^3-weighted X-ray absorption obtained by normalization and background subtraction as described earlier. Fitting parameters were N_i (N_i was not restricted to integer values), R_i, σ_i^2, and E_0. The (apparent) coordination number, N_i, gives the number of ith-type backscattering atoms at a distance R_i per absorbing atom. The function $f_i(\theta,k)$ includes the backscattering amplitude function and a damping factor, which depends on the photoelectron mean free path; $\alpha(k)$ is the phase shift for the absorber−scatterer pair due to their respective potentials. $f_i(\theta,k)$ and $\alpha(k)$ are smooth functions of k; the fitting program used tabulated values for all relevant backscatterer elements and backscatterer distances using curved-wave amplitude and phase functions calculated by McKale et al. (1988). E_0 was a fitting parameter; thus, $\chi(k)$ was rescaled during the curve-fitting process according to eq 1. The technique of data processing described earlier and the curve fitting were tested extensively on crystallographically characterized Mn-containing complexes (Guiles, 1988; Guiles et al., 1990; DeRose, 1990; DeRose et al., 1994).

The normalized error sum, Φ (sum of squared deviations between measured and calculated values), is given by the following equation:

$$\Phi = \sum_i^N (1/s_i^2)(\chi^{\text{exptl}}(k_i) - \chi^{\text{theor}}(k_i))^2 \quad (3)$$

where N is the number of data points and s_i is defined as

$$1/s_i = k_i^3/\sum_j^N k_i^3|\chi_j^{\text{exptl}}(k_j)| \quad (4)$$

The ϵ^2 error is a measure of the goodness of the fit, which takes into account the number of free-running fit parameters (p) and the number of independent data points (N_{ind}):

$$\epsilon^2 = [N_{\text{ind}}/(N_{\text{ind}} - p)]N^{-1}\Phi \quad (5)$$

The number of independent data points is estimated to be equal to $2\Delta k\Delta R/\pi$, where Δk is the k range of the data used and ΔR is the width of the Fourier-filtered peak [for further details on eq 5, see Bunker et al. (1991) and Binsted et al. (1992)]. A positive value for ϵ^2 usually indicates that the fit is not underdetermined, because the number of free parameters does not exceed the number of independent data points. (For an underdetermined fit, various sets of the p running fit parameters result in the same minimal error sum; i.e., the solution to the fit problem is not unique.) In most cases, a fit with a higher number of shells, and thus with a higher number of free parameters, results in a decrease in the Φ error (eq 3); nonetheless, ϵ^2 may increase due to the greater value of p in eq 5. A decrease in Φ alone does not justify the existence of an additional shell of backscatterer atoms (one more distinct absorber−backscatterer distance); however, an increase in ϵ^2 does not disprove the existence of an additional shell of backscattering atoms.

The ϵ^2 as calculated by eq 5 does not take into account additional constraints used by the fit program (for example, the requirement of reasonable apparent coordination numbers and restricted ranges for the ΔE_0 values). If additional constraints are applied, the ϵ^2 value as calculated by eq 5 may not be a fully appropriate parameter with which to judge the goodness of a fit. Nonetheless, in the absence of a better alternative, we have calculated ϵ^2 using eq 5. Curve fitting was achieved by minimizing the error sum as defined by eq 3. In Tables 1−3, both error sums, Φ (eq 3) and ϵ^2 (eq 5), are displayed.

RESULTS

X-ray Absorption Near-Edge Structure. The Mn K-edge spectra were recorded for three different states of NH_3-treated PS II samples: the dark-adapted state (in the following called the NH_3 S_1-state), the state illuminated at 195 K (NH_3 S_2-state), and the state illuminated at 195 K and annealed at 4 °C (annealed NH_3 S_2-state) (see Figure 1A).

The inflection point energy was determined from the zero crossing of the second derivative (Figure 1B). The following values were obtained (mean values and standard deviations of three data sets per state): NH_3 S_1-state, 6552.58 ± 0.14 eV; NH_3 S_2-state, 6553.45 ± 0.17 eV; annealed NH_3 S_2-state, 6553.63 ± 0.05 eV. We do not know whether the slight shift in the edge position upon annealing is significant. The edge positions for the NH_3 S_1-state and for both NH_3 S_2-states are similar to those of control samples not treated with NH_3. In the past, edge positions were assigned as the maximum of the first derivative (Goodin et al., 1984; Yachandra et al., 1987). Now, due to better signal to noise ratios, the more precise method of using the zero crossing of the second derivative is preferred (Liang et al., 1994).

The release of manganese from the oxygen-evolving complex of PS II leads to Mn(II), which gives rise to

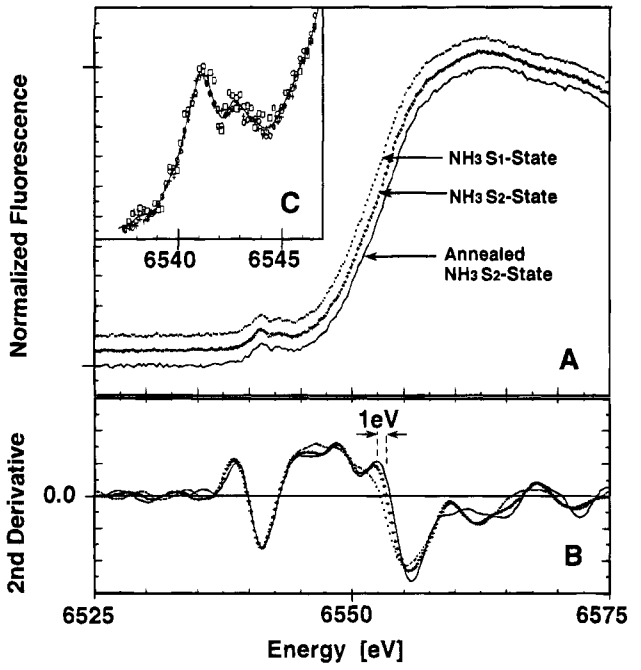

FIGURE 1: Mn K-edge spectra (A) and pre-edge spectra (C) of ammonia-treated samples. In (B) the second derivatives of the fluorescence-detected absorption spectra are shown. In (A) and (B): dots, dark-adapted sample (NH_3 S_1-state); crosses, sample illuminated at 195 K (NH_3 S_2-state); solid line, sample illuminated at 195 K and annealed at 4 °C (annealed NH_3 S_2-state). In (C) circles, NH_3 S_1; crosses, NH_3 S_2; squares, annealed NH_3 S_2; solid line, line through sum spectrum of the three data sets.

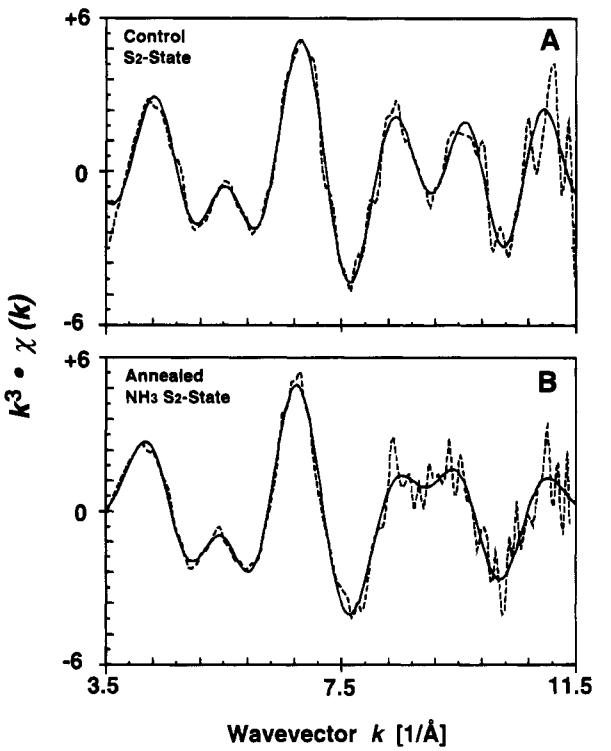

FIGURE 2: *k*-space Mn EXAFS spectra. The energy scale of the EXAFS data was transformed into a wave vector scale according to eq 2. The absorbance values are normalized to the free-atom absorption and weighted by k^3, as described in Materials and Methods. (A) PS II preparation illuminated at 195 K, no NH_3 treatment (control S_2-state). (B) Ammonia-treated PS II preparation, illuminated at 195 K and annealed at 4 °C (annealed NH_3 S_2-state). Symbols (- - -) raw data; (—) smoothed data obtained by isolation of the first three Fourier transform peaks shown in Figure 3, back-transformed into *k* space.

characteristic features in the edge spectra; the absence of these features shows that the OEC is intact under the conditions of NH_3 treatment. (This was verified by EPR measurements as well.) Upon annealing, some minor changes occur in the shape of the absorption edge, particularly in the region after the inflection point (Figure 1B). This phenomenon could be an indication of a modified nearest-ligand environment of the manganese atoms (Kusunoki et al., 1990).

The pre-edges of the ammonia-treated PS II samples are, within the limits of the signal-to-noise level, identical to those of control samples (not shown). Upon annealing of ammonia-treated samples, as shown in Figure 1C, we observe no changes in the pre-edge spectrum.

Extended X-ray Absorption Fine Structure. Mn EXAFS spectra were recorded for PS II samples in the annealed NH_3 S_2-state and for control samples (S_2-state, no ammonia treatment). The resulting k^3-weighted *k*-space spectra (for details, see Materials and Methods) are shown in Figure 2. The ammonia treatment leads to a clear (and fully reproducible) change in the *k*-space spectrum: the EXAFS oscillations for wave vectors greater than 7.5 $Å^{-1}$ are significantly damped for the annealed NH_3 S_2-state samples (Figure 2B) relative to those for control samples (Figure 2A).

The Fourier transforms of the *k*-space spectra exhibit three well-resolved peaks (peaks I–III in Figure 3). The features visible for R' greater than 3.5 Å are not reproducible; they result from high-frequency noise components in the *k*-space spectrum. The three resolved peaks represent the backscattering of photoelectrons by atoms at a distance *R*. Thus, each of the three resolved peaks corresponds to backscattering shells of the absorbing manganese atoms. Due to the averaged phase shift for the absorbing–scattering pairs of

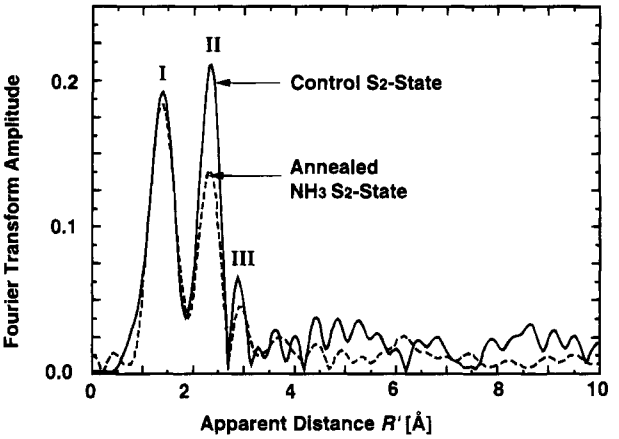

FIGURE 3: Fourier transforms of the *k*-space data of Figure 2. Each peak represents one coordination shell of the absorbing manganese atoms at a distance of approximately $R' + 0.5$ Å.

atoms, the apparent distance R' is generally less than *R* by 0.2–0.5 Å.

The 2.7 Å Coordination Shell. The most pronounced effect of the ammonia treatment on the EXAFS Fourier-spectrum is a decrease in the amplitude of the second peak. The amplitude of a Fourier peak depends on the corresponding coordination number and also on the degree of disorder or heterogeneity within the coordination shell. The peak amplitude increases with increasing coordination number, due to the additive superposition of EXAFS oscillations of individual atoms of the coordination shell. But whenever

EXAFS oscillations of similar atoms with slightly different distances from the absorbing atom are superimposed, the magnitude of the Fourier peak is diminished due to a frequency difference between the EXAFS oscillations of the atoms at different distances, which results in destructive interference of the two superposed EXAFS oscillations; the decreased magnitude of the *k*-space EXAFS oscillations corresponds to a decreased amplitude of the Fourier peak.

Differences in distance may arise from dynamic disorder (vibrations of atoms) or static disorder (an ensemble of frozen conformational substates). In current EXAFS theories these phenomena are considered; by assuming a Gaussian distribution of distances, a Gaussian-type damping of the *k*-space oscillation is predicted, which is characterized by a damping constant σ, the Debye−Waller factor (Teo, 1986; see eq 2). However, different internuclear distances contributing to one Fourier peak can also be due to discrete heterogeneity arising from two distinct types of Mn−Mn binuclear centers with slightly different internuclear distances.

The second peak represents manganese backscattering from (at least) two di-μ-oxo-bridged manganese binuclear moieties with a Mn−Mn distance of about 2.7 Å (Yachandra et al., 1986, 1987; DeRose, 1990; Sauer et al., 1992). In the ammonia-treated samples, the second peak is decreased in comparison to the second peak of control samples by 35−40% (Figure 3). The Mn K-edge data provide evidence against dramatic changes in the structure, such as the release of manganese or changes in the symmetry of the metal centers upon treatment with ammonia. Therefore, ammonia-induced changes in coordination numbers are not a likely cause of the decrease in the second peak. The more likely origin is the occurrence of significant heterogeneity within the backscattering paths contributing to the second Fourier peak, for example, due to an ammonia-induced change in the Mn−Mn distance of one distinct manganese binuclear cluster of the OEC. As discussed earlier, such heterogeneity should lead to a more pronounced damping of the *k*-space EXAFS oscillations at higher wavenumbers. Indeed, after the second peak is isolated and back-transformed into *k* space, the EXAFS oscillations of the ammonia-treated sample are significantly damped at higher wavenumbers in comparison to the respective oscillations of the control sample with no NH_3 treatment (see Figure 4A).

The data resulting from Fourier isolation of the second peak were subjected to curve fitting using the function given by eq 2 with amplitude and phase functions for Mn as the absorbing and the backscattering atom. Two different approaches were used. A one-shell fit was accomplished by using only one term of the sum expression in eq 2. This fit resulted in parameters shown in the upper part of Table 1. One data set (superscript *b*) that was used for the curve fitting resulted from the weighted addition of two energy space spectra of one oriented sample; the other two data sets were obtained by measurements of isotropic samples. The distance, *R*, and the coordination number, *N*, determined for the annealed NH_3 S_2-state are not different from the respective values for the untreated control S_2-state (Table 1). However, we observe an increased Debye−Waller factor in comparison to those of control samples. As discussed earlier, the increase in the Debye−Waller factor could result from the appearance of heterogeneity among the distances of the second coordination shell, mimicking increased disorder (Teo, 1986).

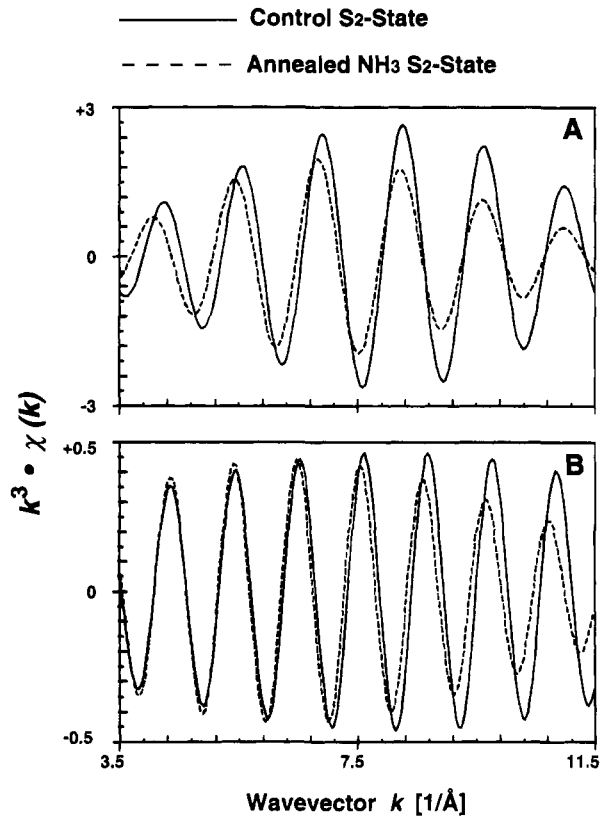

FIGURE 4: *k*-space data corresponding to the second (A) and third (B) Fourier peaks of Figure 3. After Fourier transformation, the second and third peaks were isolated by applying a window function $\Delta R = 1.0-1.2$ and 0.6−0.8 Å, respectively, and back-transformed into *k* space. The resulting EXAFS oscillations represent the backscattering from the atoms of the respective coordination shell only.

Because a discrete heterogeneity of distances appears to be a likely origin for the observed decrease in the second Fourier peak, the data sets were also fit under the assumption that two different Mn−Mn distances contribute to the second Fourier peak (two subshells). Thus, two terms of the sum in eq 2 were used to fit the Fourier-isolated data. As seen in the lower part of Table 1, this fit approach leads to a decrease in the error sum by 45−65%. However, the presence of eight free parameters leads to minima in the error sum for a variety of different solution sets. Therefore, we decided to decrease the degrees of freedom by using two physically reasonable restrictions. First, we assumed the disorder for the individual subshells to be equal ($\sigma = \sigma_1 = \sigma_2$), and second, we required the difference in the ΔE_0 values of the two scatter shells to be small, i.e., <3 eV. This restriction is reasonable because the ΔE_0 mainly depends on the properties of the absorbing and backscattering atoms; the respective atoms are assumed to be identical for the two subshells, although different oxidation states may be involved. Under these assumptions a unique solution was found for each data set. Excellent curve-fitting results were obtained for $0.001 < 2\sigma^2 < 0.003$. Note that this is significantly smaller than the Debye−Waller factors for the one-shell fits. We chose a value of 0.002 for $2\sigma^2$; the curve-fitting results are shown in the lower part of Table 1. The ϵ^2 value of the two-shell fit is not negative (thus there is no indication that the fit is underdetermined), but it is clearly higher than the ϵ^2 value of the one-shell fit. (For a definition of ϵ^2 and the meaning of the ϵ^2 increase, see Materials and

Table 1: Mn EXAFS Fit Parameters for Annealed NH_3 S_2 and Control S_2 for Fourier Peak II[a]

	One Mn−Mn Distance					
sample	R (Å)	N	$2\sigma^2$ (Å^2)	ΔE_0 (eV)	Φ ($\times 10^3$)[f]	ϵ^2 ($\times 10^5$)[f]
annealed NH_3 S_2						
(1)	2.71	1.1	0.012	−9	0.51	0.46
(2)	2.73	1.4	0.013	−17	0.33	0.30
(3)[b]	2.74	1.3	0.013	−16	0.53	0.68
⟨average⟩[c]	2.72	1.26	0.013			
stand. dev[d]	±0.01	±0.14	±0.001			
⟨control S_2⟩[c]	2.73	1.26	0.006			
stand. dev	±0.02	±0.15	±0.001			

	Two Mn−Mn Distances							
sample	R_1 (Å)	R_2 (Å)	N_1	N_2	$\Delta E_{0(1)}$ (eV)	$\Delta E_{0(2)}$ (eV)	Φ ($\times 10^3$)[f]	ϵ^2 ($\times 10^5$)[f]
annealed NH_3 S_2								
(1)	2.71	2.86	0.7	0.4	−13	−11	0.18	1.16
(2)	2.71	2.85	0.8	0.6	−14	−13	0.15	0.95
(3)[b]	2.72	2.86	0.7	0.5	−13	−11	0.29	1.87
⟨average⟩[c]	2.71	2.86	0.74	0.5				
stand. dev[d]	±0.01	±0.01	±0.04	±0.07				

[a] Fit parameters are as defined in the text. For two-shell fits, shells 1 and 2 are both Mn−Mn. [b] This data set was calculated from the weighted addition of normalized data measured on a partially oriented sample at 10° and 80° detection angles (normalized E-space data weighted by 0.33 and 0.66, respectively). [c] Mean values of the fit results of three data sets. [d] Standard deviations of the mean values. [e] The Debye−Waller factors for both subshells were fixed: $2\sigma_1^2 = 2\sigma_2^2 = 0.002$ Å^2. [f] The goodness of fit parameters Φ and ϵ^2 are defined in Materials and Methods.

Methods and Discussion.) The standard deviations for all fit parameters are relatively small, reflecting a high degree of reproducibility.

A two-shell fit of the control data sets (control S_2-state, no NH_3 treatment) under the same restrictions did not show significant improvement. It resulted in a very low coordination number for the second shell (< 0.1); the error sum was only slightly lower (by about 25%) than that for the one-shell fit.

In conclusion, the parameters resulting from the two-shell fit of the annealed NH_3 S_2-state samples are indicative that ammonia binding to the manganese complex results in an increase in some Mn−Mn distances from 2.72 to 2.87 Å. We assume that in the untreated PS II there are two dissimilar 2.7 Å Mn−Mn binuclear moieties (see Discussion). One of these moieties is affected by ammonia treatment, lengthening the Mn−Mn distance to 2.87 Å; the distance for the other is unchanged at 2.72 Å (average of values from curve-fitting results is shown in Table 3).

The 3.3 Å Coordination Shell. The third peak in the Fourier spectrum of the annealed NH_3 S_2-state samples clearly is decreased in amplitude in comparison to the corresponding peak in the spectrum of the control S_2-state samples with no NH_3 treatment (see Figure 3). In analogy to the decreased second Fourier peak, the Fourier-isolated k-space data exhibit increased damping at higher wavenumbers, most likely due to increased heterogeneity within the third coordination shell of the absorbing manganese atoms (Figure 4B). Curve fitting under the assumption of a homogeneous coordination shell of Mn at 3.3 Å results in an increased Debye−Waller factor of the ammonia-treated samples in comparison with control samples (Table 2). This behavior was observed in all ammonia-treated samples. Therefore, it is unlikely that the decreased peak height is due to a random superposition of noise and third-peak EXAFS oscillations. The increased Debye−Waller factor is also observed for a joint fit of the Fourier-isolated second and third peaks using the fit approach proposed by DeRose et al. (1994; results not shown).

Table 2: Mn EXAFS Fit Parameters for Annealed NH_3 S_2 and Control S_2 for Fourier Peak III[a]

	One Mn−Mn Distance					
sample	R (Å)	N	$2\sigma^2$ (Å^2)	ΔE_0 (eV)	Φ ($\times 10^3$)[e]	ϵ^2 ($\times 10^5$)[e]
annealed NH_3 S_2						
(1)	3.30	0.68	0.016	−12	0.30	0.67
(2)	3.39	0.68	0.017	−7	0.42	0.99
(3)[b]	3.38	0.56	0.013	−3	0.09	0.20
⟨average⟩[c]	3.35	0.64	0.013			
stand. dev[d]	±0.04	±0.06	±0.001			
⟨control S_2⟩[c]	3.33	0.4	0.004			
stand. dev.[d]	±0.01	±0.12	±0.002			

[a] Fit parameters are as defined in the text. [b] This data set was calculated from the weighted addition of normalized data measured on a partially oriented sample at 10° and 80° detection angles (normalized E-space data weighted by 0.33 and 0.66, respectively). [c] Mean values of the fit results of three data sets. [d] Standard deviations of the mean values. [e] The goodness of fit parameters Φ and ϵ^2 are defined in Materials and Methods.

The 1.9 Å Coordination Shell. For annealed NH_3 S_2-state samples, the 1.9 Å Fourier peak does not show fully reproducible differences in comparison to the 1.9 Å peak of control samples. The decreased peak height visible in Figure 3 was found for most, but not all, ammonia-treated samples. Fits of the Fourier-isolated first peak of ammonia-treated samples did not result in parameters clearly different from those of control samples with no NH_3 treatment (Yachandra et al., 1986; DeRose, 1990; Guiles et al., 1990; MacLachlan et al., 1992; Liang et al., 1994).

EPR Analysis of Partially Oriented EXAFS Samples. PS II membrane particles were oriented on Mylar tape as described in Materials and Methods. This technique results in a preferred orientation of the PS II-containing membrane parallel to the Mylar support. To assess the extent of orientation achieved, the angle dependence of the X-band EPR signals of the oxidized cytochrome b_{559}, which is part of the PS II complex, was analyzed.

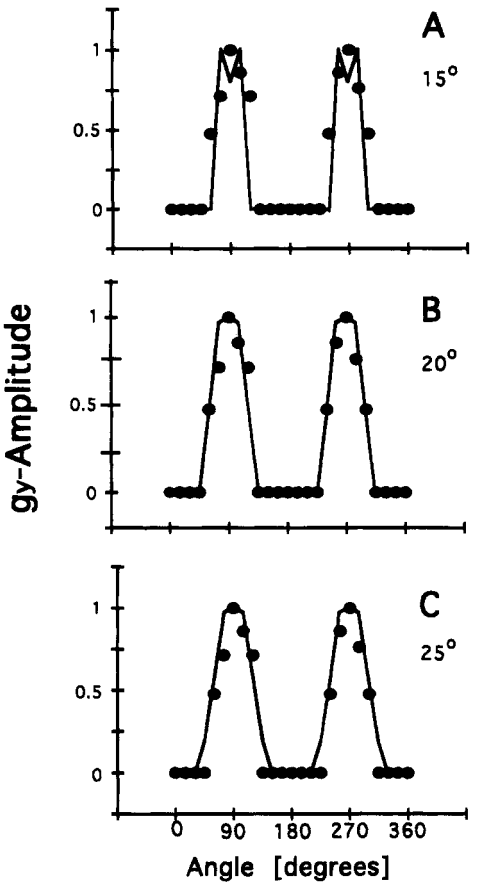

FIGURE 5: Orientation dependence of the g_y EPR signal of the oxidized cyt b_{559}. The normalized amplitude of the first derivative of the g_y signal is shown versus the detection angle. The filled circles give the experimentally determined g_y amplitude, and the solid line represents the amplitudes simulated for different disorder angles: $A = 15°$, $B = 20°$, $C = 25°$.

The angle dependence of the cyt b_{559} of partially oriented thylakoid membranes has been previously described (Rutherford, 1985). In this study, we evaluate the angle dependence of the g_y and g_z EPR signals of the cyt b_{559} in a quantitative way to determine the degree of orientation obtained. There was no detectable shift in the position of the g_y or g_z signal (not shown), indicating that perfect orientation was not obtained (Blum et al., 1978). The amplitude of the g_y signal approaches zero for an angle of 0° and is at a maximum at 90° between the magnetic field and the Mylar tape normal (see Figure 5). This finding establishes that there is no significant fraction of PS II particles that are unoriented. By assuming a Gaussian distribution of the angle between the thylakoid membrane normal and the Mylar tape normal, the angle dependence of the amplitudes of the g_y and g_z signals was simulated as described by Blum et al. (1978). For the data set shown in Figure 5, the best agreement between simulations and experimental results was obtained for a half-width of the Gaussian distribution function of 20° (see Figure 5). The mosaic spread of the angles estimated by comparison of the cyt b_{559} g_y signal with simulations was used for the quantitative interpretation of EXAFS data, as described in the following.

X-ray Absorption Measurements on Partially Oriented PS II. For oriented annealed NH_3 S_2-state samples, Mn K-edge spectra were recorded for different angles between the X-ray electric field vector and the membrane normal. A pronounced angle dependence of the edge spectra was observed (data not shown). The angle dependence of the shape of the edge spectra and the pre-edge was similar to that found for samples not treated with ammonia (Mukerji et al., 1994). This finding indicates that no major structural rearrangements are induced by the ammonia treatment. In particular, the edge spectra did not exhibit features characteristic of Mn(II); the ammonia treatment and orientation procedure did not result in any detectable release of Mn(II).

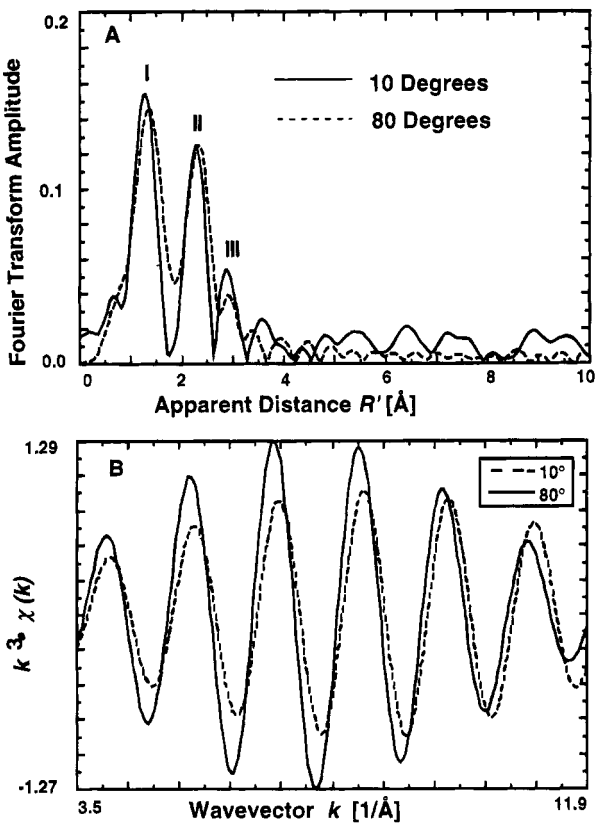

FIGURE 6: (A) Fourier transforms of the EXAFS for oriented PS II samples in the annealed NH_3 S_2-state. The solid and broken lines are from two data sets measured with an angle between the PS II membrane normal and the X-ray electric field vector of 10° and 80°, respectively. (B) *k*-space isolates of the second Fourier peak of oriented ammonia-treated PS II. The isolation procedure is described in the caption to Figure 4.

For angles of 10° or 80° between the membrane normal and the X-ray electric field vector, **e**, EXAFS data were recorded and processed as described earlier. The 10° and 80° data sets exhibit clear differences in the *k*-space spectra (not shown), which result in differences in the Fourier transforms (Figure 6A). In particular, the magnitude of the third Fourier peak is clearly greater at 10° and the second Fourier peak is broadened at 80°. In *k* space, both Fourier-isolated peaks exhibit a clear orientation dependence of the damping (Figure 6B). For a single absorber−backscatterer vector, the damping should not exhibit a pronounced orientation dependence. Thus, this orientation dependence of the shape of the Fourier-isolated EXAFS oscillations suggests that the individual Fourier peaks result from a superposition of EXAFS oscillations arising from scattering atoms at two (or more) different distances and with different orientations with respect to the membrane normal.

The Fourier-isolated second-peak data were subjected to curve fitting using the same approaches described earlier for the nonoriented samples. For some data sets, it was

Table 3: Mn EXAFS Fit Parameters for Oriented Annealed NH_3 S_2-State at Different Angles for Fourier Peak II[a]

	Two Mn−Mn Distances[b]							
angle θ[d] (deg)	R_1 (Å)	R_2 (Å)	$N(\theta)_1$	$N(\theta)_2$	$\Delta E_{0(1)}$ (eV)	$\Delta E_{0(2)}$ (eV)	Φ ($\times 10^3$)[c]	ϵ^2 ($\times 10^5$)[c]
10	2.73	2.89	0.68	0.28	−13	−13	0.19	1.14
10	2.72	2.88	0.74	0.32	−16	−9	0.22	1.37
10	2.73	2.88	0.66	0.34	−14	−7	0.12	0.74
54.7[e]	2.71	2.86	0.75	0.50	−14	−12	0.17	1.06
70	2.75	2.89	0.90	0.56	−11	−10	0.12	0.74
80	2.73	2.86	0.76	0.62	−15	−14	0.15	0.92

[a] Fit parameters are as defined in the text. Two-distance fits (1 and 2) are both Mn−Mn. [b] The following restriction has been applied to the Debye−Waller factors of both subshells: 0.003 Å^2 ≥ $2\sigma^2$ ≥ 0.001 Å^2. [c] The goodness of fit parameters Φ and ϵ^2 are defined in Materials and Methods. [d] The angle between the membrane normal of the oriented PS II sample and the X-ray **e** vector is given. [e] The average of two values are data (two-distance fits) from two unoriented samples from Table 1.

necessary to allow a difference in the ΔE_0 values of up to 7 eV to obtain good fits. The parameters obtained are given in Table 3. The apparent coordination numbers for the 2.87 Å distance show a clear orientation dependence.

The angle dependence of the apparent coordination numbers, $N(\theta)$ (Figure 7), was fit to the equation $N(\theta) = F_{ab}(\theta)N_{iso}$, where $N(\theta)$ is the coordination number at angle θ and N_{iso} is the coordination number for an (hypothetical) unoriented sample, which is assumed to be identical to the apparent coordination number for an oriented sample with $\theta = 54.7°$, the magic angle, and

$$F_{ab}(\theta) = \frac{3[\int_{\phi=0}^{\pi}(^1/_2 \sin^2\theta \sin^2\phi + \cos^2\theta \cos^2\phi)\, p(\phi)\, d\phi]}{\int_{\phi=0}^{\pi} P(\phi)\, d\phi} \quad (6)$$

where ϕ is the angle between the Mylar plane normal and the absorber−backscatterer ($\vec{ab}$) vector, θ is the angle between the X-ray **e**-vector and the membrane normal, and $P(\phi) = \sin\phi \exp[-(\ln 2)(\phi - \phi_{ab})^2/\Omega^2]$ is the probability that the $\vec{ab}$ vector has the orientation ϕ. Deviations from perfect orientation of the membrane sheets are considered by assuming a Gaussian distribution of angles around ϕ_{ab}, with Ω being the mosaic spread.

The orientation disorder obtained by the paint and dry procedure was not identical for all samples. On the basis of the orientation dependence of the cyt b_{559} EPR signals, we estimated that it was between 20° and 30° for all samples. Therefore, a mean value of 25° has been used for the fit shown in Figure 7. Variation in Ω by 5° results in a change of $\phi_{2.87}$ by less than 1.5°; for $\phi_{2.72}$ the influence is even smaller (the subscripts 2.72 and 2.87 refer to each of the two Mn−Mn vectors, one at $R = 2.72$ Å; and one at $R = 2.87$ Å: average values obtained from Table 3). The individual angles of the two absorber−scatterer distances with respect to the membrane were obtained by means of a least-squares fit of the angle dependence of the apparent coordination number. This was achieved by a fit of $N(\theta)$ vs θ to eq 6. The resulting angles ($\phi_{2.72}$ and $\phi_{2.87}$) and coordination numbers ($N_{2.87}$ and $N_{2.72}$) are given in Figure 7. For the 2.87 Å distance as well as the 2.72 Å distance, the resulting coordination numbers, $N_{2.87}$ and $N_{2.72}$, are almost identical to the respective coordination numbers found for nonoriented samples (Table 1). This consistency confirms that the orientation procedure does not result in a change in the structure of the manganese complex.

For all samples studied, the magnitude of the third Fourier peak (3.3 Å interaction) showed a similar orientation dependence; the peak amplitude was maximal at 10° and usually minimal at 70° or 80°. However, the third peak for the 70° and 80° data sets is very close to the noise level (see Figure 6). Probably due to noise problems, the results of two-shell fits for different oriented data sets were not fully consistent. More data and better data evaluation techniques are required to determine the angles between the membrane normal and the individual absorber−backscatterer distances contributing to the third peak. With regard to the first Fourier peak, it is likely that 24 Mn−O or Mn−N interactions contribute to this peak. Therefore, the determination of angles for the individual absorber−backscatterer interactions is not feasible.

DISCUSSION

X-ray Absorption Near-Edge Structure. The position of the inflection point and the shape of Mn K-edge spectra depend mainly on the oxidation state of the absorbing atom, but position and shape are also modified by the ligand environment (Kusunoki et al., 1990; Penner-Hahn et al., 1990). The Mn K-edge spectra of the NH_3 S_1-state and the NH_3 S_2-state (Figure 1A) closely resemble the respective spectra of samples not treated with NH_3 [not shown; for comparison, see Sauer et al. (1988) and Yachandra et al. (1993)]. It is important to note that illumination at 195 K shifts the inflection points of the NH_3-treated samples to higher energies by about 1 eV. This indicates that the light-induced manganese oxidation that occurs upon the S_1 to S_2 transition is not affected by NH_3 treatment. Apparently the annealing procedure does not result in a further change in the Mn oxidation state. The minor change of about 0.2 eV observed between the average edge position for the NH_3 S_2-state and the annealed NH_3 S_2-state may result from a change in the Mn ligand environment. MacLachlan et al. (1994) have also conducted Mn K-edge studies of ammonia-treated PS II. They found edge energies that are significantly lower than those reported in this study for both the S_1 and annealed S_2 states.

The weak pre-edge visible at about 6541 eV in Figure 1C arises from electronic transitions from 1s to unfilled 3d levels. These transitions are weak, because they are formally dipole-forbidden. They gain intensity from mixing with p-type orbitals or due to the presence of a significant quadrupole transition moment. Therefore the position, width, and magnitude of this pre-edge are highly sensitive to changes in the symmetry of the ligand environment (Shulman et al., 1976; Kusunoki et al., 1990). Upon the annealing of ammonia-treated samples, as shown in Figure 1C, we observe no changes in the pre-edge spectrum. We can therefore conclude that the symmetry properties of the manganese metal centers seem to be unmodified by the ammonia treatment.

Extended X-ray Absorption Fine Structure. The binding of ammonia in the S_2-state of the OEC (annealed NH_3 S_2-state) causes obvious changes in the EXAFS spectra. These changes are relevant to the question of whether and where

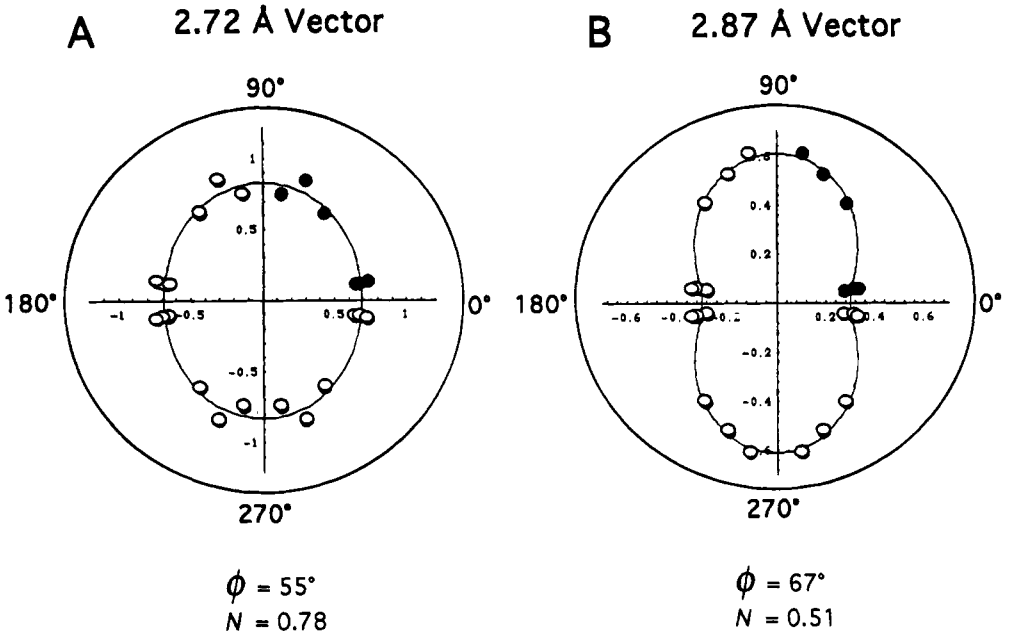

FIGURE 7: Angle dependence of the apparent coordination numbers. The apparent coordination numbers, $N(\theta)$, given in Table 3 are plotted vs the detection angle in the form of a polar diagram. The solid line has been obtained by fitting the experimental data to eq 6 with Ω = 25° using a least-squares error criterion. Solid circles are data from three oriented samples and one unoriented sample. The open circles are data points that have been mirrored for clarity. The error ranges were determined as the parameter values for which the error sum increased by 100%. The resulting average angles with respect to the membrane normal and isotropic coordination numbers are reported: $\phi_{2.87} = 67° \pm 3°$, $N_{2.87} = 0.51 \pm 0.04$; $\phi_{2.72} = 55° \pm 4°$, $N_{2.72} = 0.78 \pm 0.09$.

NH_3 or NH_3 derivatives ligate to the Mn atoms of the OEC. Equally important, however, is the resolution of the average angle problem in EXAFS dichroism studies due to the modification of the OEC by ammonia binding. Both aspects are discussed in the following.

Ammonia-Induced Heterogeneity in the Second Fourier Peak at 2.7 Å. Guiles et al. (1990) described a heterogeneity of the 2.7 Å Mn−Mn distances in the S_3-state; DeRose (1990) found evidence for a less pronounced, but qualitatively similar, effect resulting from fluoride treatment (DeRose et al., 1995). Liang et al. (1994) observed distance heterogeneity for the Mn complex in the S_2 state that gives rise to an EPR signal at $g \sim 4$.

In the annealed NH_3 S_2-state, the EXAFS oscillations that correspond to the second Fourier peak are more clearly damped than those of control samples not treated with ammonia (Figure 4A). In principle, there are two possible explanations for this phenomenon: (i) the disorder of all 2.7 Å Mn−Mn moieties is increased (increased width of the Gaussian distance distribution) or (ii) a distance change occurs in a fraction of these moieties, resulting in two distinct Mn−Mn distances that are close to 2.7 Å (distance heterogeneity). For these two models of the ammonia effect on the EXAFS spectrum, parameters were determined by curve-fitting (one-shell and two-shell fits in Table 1). The one-shell approach is suggestive of an ammonia-induced increase in the Debye−Waller factor. The two-shell fit indicates that the decrease in the second Fourier peak could result from an ammonia-induced lengthening of 40% of the Mn−Mn moieties by ~0.15 Å (two-shell fit in Table 1). The transition from the one-shell fit to the two-shell fit results in a decrease in the error sum (Φ error), but not in the ϵ^2 value (for the definition and meaning of ϵ^2, see Materials and Methods). The increase in ϵ^2 indicates that the decrease in Φ alone is not a conclusive argument for a two-shell vs a one-shell fit of the data. We can supplement the argument against the one-shell approach (decreased disorder of all Mn−Mn moieties) and in favor of the two-shell approach (distance heterogeneity model) as follows.

(1) Presumably the 2.7 Å Mn−Mn distance is due to a di-μ-oxo bridge between two Mn atoms (Sauer et al., 1992; Klein et al., 1993; Yachandra et al., 1993). It is difficult to imagine any mechanism that results in an ammonia-induced increase in the width of the Gaussian distance distribution (= Debye−Waller factor) for such a relatively rigid structure. In other words, we consider the assumption of a considerably increased Debye−Waller factor for the 2.7 Å Mn−Mn distance to be physically unreasonable.

(2) The two-shell approach is based on the assumption that there are two distinct 2.7 Å binuclear Mn moieties per PS II. This assumption is well-supported by experimental results as reviewed elsewhere (Debus, 1992; Sauer et al., 1992; Klein et al., 1993). Presumably, at least with respect to their redox states, these two Mn moieties are inequivalent. Further evidence for two chemically distinct 2.7 Å Mn−Mn moieties comes from studies of hydroxylamine-treated PS II in the S_0-state (Riggs et al., 1993). In these studies, one of the 2.7 Å Mn−Mn binuclear units dissociated upon treatment, leaving the other intact. This reinforces the proposal that the two Mn−Mn binuclear units in PS II are in different chemical environments. Thus, it is possible that ammonia treatment specifically affects one of the two inequivalent Mn−Mn units.

(3) There is considerable evidence that the so-called second ammonia binding site (SY II) is related to the ligation of ammonia to manganese (see introduction); it is likely that SY II is located specifically at one of two inequivalent binuclear Mn moieties. A small distance change in the respective binuclear Mn moiety is a possible consequence.

(4) The EXAFS measurements of oriented PS II samples indicate that the damping of the second-peak oscillations (see Figure 3B) depends on the detection angle. This pronounced

angle-dependent damping clearly is not in agreement with the assumption of an increased Debye−Waller factor for all 2.7 Å Mn−Mn moieties involved. It is, however, in agreement with the assumption that there are two dissimilar Mn−Mn binuclear units contributing to the second Fourier peak, of which only one is affected by ammonia binding; the Mn−Mn vector of the binuclear unit that is affected, with length $R = 2.87$ Å, is at an angle of 67°, whereas the second vector, with length $R = 2.72$ Å, is at an angle of 55°.

Because of the preceding statements, we assume that the two-shell approach is appropriate for the manganese complex in the annealed NH_3 S_2-state. We conclude that the Mn−Mn binuclear moieties that are assumed to constitute the Mn complex in the S_2-state are dissimilar in such a way that the structure of only one Mn−Mn binuclear unit is affected by ammonia binding. The dissimilarity in the Mn oxidation states of the two moieties, i.e., Mn_2(III,IV) vs Mn_2(IV,IV) in the S_2-state (Yachandra et al., 1992), might be the factor that is crucial for the differential response of the two binuclear units to ammonia. It is probable that steric factors play an important role, as indicated by the specificity of ammonia binding at the second NH_3 site, which is not accessible to larger amines.

We reiterate that a two-shell fit is preferred over a one-shell fit on the basis of chemical and physical reasonableness and not solely on the basis of Φ or ϵ^2 values. Further studies are underway to address the question of heterogeneity in the second peak observed in NH_3-treated samples, F^--treated samples, and samples characterized by the $g = 4.1$ EPR signal, and the details will be the subject of a future publication.

Ammonia-Induced Heterogeneity in the Third Fourier Peak at 3.3 Å. In the annealed NH_3 S_2-state, the third EXAFS Fourier peak is decreased in comparison with that of control samples not treated with ammonia (Figure 3). This experimental result is fully reproducible and therefore not explainable by random noise contributions. The decreased height of the third Fourier peak is especially obvious at the 10° and 15° orientations [compare Figure 6 with Figure 5 of Mukerji at al. (1994)]. At this orientation, the third-peak amplitude is enlarged compared to the noise level.

Figure 4B and the fit results shown in Table 2 suggest that the decreased amplitude is the consequence of increased damping of the third-peak EXAFS oscillation (Figure 4B, Table 2). In analogy with our discussion of the second Fourier peak, we conclude that the most likely reason for the decreased third Fourier peak is distance heterogeneity. Thus, the experimental result can be taken as an indication that at least two absorber−backscatterer interactions contribute to the corresponding EXAFS oscillations.

The origin of the ammonia effect on the third EXAFS peak may be clarified by the use of a more detailed fit approach (two or three subshells). To avoid an underdetermined fit, the use of constraints that are derived from a structural model is essential for any multishell fit of the third-peak EXAFS data. In contrast with the second EXAFS peak, a two-shell fit of the third peak is difficult to justify because of three problems: (1) it is still unclear what model to use (i.e., what elements and how many absorber−backscatterer interactions); (2) errors in the fit results due to noise in the data become a serious problem; and (3) effects of the Fourier isolation procedure on the EXAFS data, which are possible due to the proximity of the clearly higher second peak, may result in misleading fit results.

Ligation of NH_3 to Mn. According to Britt et al. (1989), the results of electron spin echo envelope modulation studies indicate the direct coordination of an ammonia ligand to the Mn complex; an amido (NH_2) bridge between two metal ions was suggested. As discussed in the following, the observed elongation of one Mn−Mn distance by about 0.15 Å provides some evidence that the NH_3 ligand is a bridging ligand between two manganese atoms.

Amido bridges between transition metals are not uncommon in inorganic chemistry (Cristoph et al., 1969; Flood et al., 1973; Kretschmer & Heck, 1982; Heck et al., 1988). However, we are not aware of any synthetic complex containing Mn binuclear centers that are bridged by one mono-μ-oxo bridge and one amido bridge. Therefore, at the present, direct comparison of the observed changes in the X-ray absorption spectra with data from a suitable model compound is not possible. Nonetheless, some predictions are possible. By substituting μ-O with μ-NH_2, the donation of electron density to the metal centers is decreased. It seems likely that, consequently, the Mn−Mn separation is increased. In that context it is interesting to note that the protonation of a single μ-oxygen of a di-μ-oxo-bridged Mn binuclear moiety results in a lengthening of the Mn−Mn distance from 2.71 to 2.81 Å (Larson et al., 1992). The NH_2 bridging ligand, which is isoelectronic with an OH bridge, could result in a similar elongation. In contrast, for most synthetic metal complexes the Mn−Mn distance is about 2.7 Å for all di-μ-oxo-bridged Mn dimers, irrespective of the nature of the terminal ligands (Wieghardt, 1989). Therefore, we consider it less likely that an exchange of ligands that are not part of the di-μ-oxo bridges could result in an increase in the Mn−Mn distance by 0.15 Å.

Because the ligand exchange reaction occurs in the S_2-state, but not in the S_1-state, it seems likely that the increase in the Mn oxidation state is the factor that gives rise to the binding in the S_2-state. Assuming the validity of the Mn oxidation states proposed by Yachandra et al. (1993), we propose that the NH_3 ligand binds to the Mn(III)−Mn(IV) binuclear cluster in the S_2 state, which is the unit that is oxidized from Mn(III)−Mn(III) to Mn(III)−Mn(IV) accompanying the S_1 to S_2 transition. According to this proposal, the Mn−Mn binuclear center, which is characterized by an angle of 67° ± 3°, becomes oxidized and is also the site of NH_3 binding. Mukerji et al. (1994) found evidence in oriented PS II that, upon the S_1 to S_2 transition, oxidation of a Mn(III)−Mn(III) binuclear center occurs in the 2.7 Å Mn−Mn vector with an angle greater than 60°.

Ammonia Treatment of the Mn Complex as a Method for Structure Determination. As judged from the Mn K-edge spectra, pre-edge spectra, and EXAFS, ammonia treatment does not result in a major structural rearrangement of the manganese complex. No manganese is released, nor is any change detectable in the manganese oxidation state, the symmetry of the manganese ligand environment, or the stoichiometry of atoms constituting the individual coordination shells. The geometry of the ammonia-modified manganese complex seems to closely resemble that of the unperturbed complex. This conclusion is strengthened by the results of Mukerji et al. (1994), who have determined an average angle of 60° for the 2.7 Å distance of untreated PS II in the S_1- and S_2-states. In that study, however, the

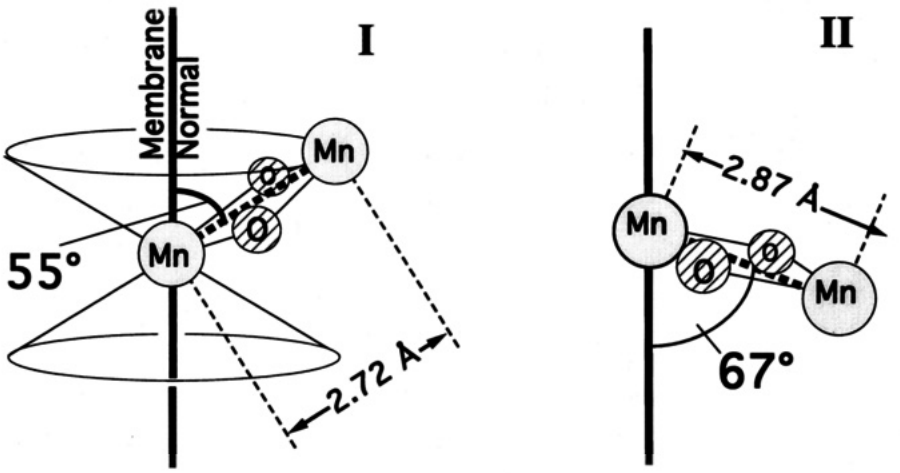

FIGURE 8: Building blocks for a structural model of the PS II manganese complex. The Mn−Mn distances and the angles with respect to the membrane normal were determined for the NH_3-treated Mn complex. The orientations of the individual Mn binuclear clusters are not uniquely determined by the experimental results; each angle corresponds to a double cone of possible orientations, as indicated in part I of this figure.

two vectors in the second peak were not resolved. For the untreated Mn complex, the average angle of 60° is in agreement with the mean of the two angles found in the NH_3-treated Mn complex. This mean angle was calculated from the individual angles and coordination numbers of the two resolved vectors using the following equation from George et al. (1993):

$$\cos^2(\phi_{av}) = \{N_{2.72}\cos^2(\phi_{2.72}) + N_{2.87}\cos^2(\phi_{2.87})\}/\{N_{2.72} + N_{2.87}\} \quad (7)$$

In conclusion, it seems likely that orientations determined for different Mn−Mn distance vectors of ammonia-treated samples are similar or identical to the respective orientations of the untreated oxygen-evolving complex.

As discussed earlier, in the annealed NH_3 S_2-state the distance degeneracy within the second Mn coordination shell is at least partially removed by the structural perturbation that results from ammonia treatment; by using an appropriate curve-fitting approach, two slightly different distances of 2.72 and 2.87 Å can be resolved. Ammonia treatment seems to be a suitable method to resolve the EXAFS interactions of individual Mn−Mn binuclear centers of the OEC. The resolution of individual EXAFS interactions is necessary to determine the orientation angle of the respective vector by EXAFS dichroism spectroscopy. Thus, ammonia treatment is one method that could help master the average angle problem of EXAFS dichroism studies mentioned in the introduction.

Structure and Orientation of the Mn complex. Assuming that the 2.7 Å Mn−Mn interaction results from a di-μ-oxo-bridged Mn binuclear cluster, we obtain the building blocks for a structural model of the PS II Mn complex in the S_2-state and for its orientation with respect to the membrane (Figure 8). At present, we cannot give an unambiguous answer to the question of how to arrange these building blocks. The proposed Mn−Mn interactions at 3.3 Å and EPR results [reviewed by Rutherford et al. (1992), Debus (1992), and Sauer et al. (1992)] are indicative that the two di-μ-oxo-bridged Mn−Mn binuclear moieties shown in Figure 8 are linked to each other. Thus, there seem to be two distinct types of possible arrangements for the building blocks of Figure 8: (1) two separate di-μ-oxo-bridged Mn binuclear units are close to each other, possibly connected by a mono-μ-oxo bridge (dimer of dimers model), or (2) the two di-μ-oxo-bridged Mn−Mn blocks are merged into a Mn−(μ_2-O)$_2$−Mn−(μ_2-O)$_2$−Mn structure and the remaining fourth Mn is connected to one of the Mn atoms by a mono-μ-oxo bridge.

Yachandra et al. (1993) proposed that the two di-μ-oxo-bridged Mn clusters are connected via a mono-μ-oxo, dicarboxylato bridge between two Mn atoms. Furthermore, Yachandra et al. proposed a cis conformation for the resulting Mn tetranuclear complex with the open side of the C-shaped structure roughly parallel to the membrane normal. The vectors from Figure 8 were arranged in the approximate configuration of this model, and the resulting structure was rotated with respect to the membrane normal until the angles given in Figure 9 were reached.

Figure 9 shows a possible orientation of the structure proposed by Yachandra et al. (1993). The two angles for the 2.7 Å Mn−Mn distances given in Figure 9 (57° and 68°) are close to the experimentally determined angles of 55° and 67°. (Perfect agreement between calculated angles and the experimentally determined ones was not obtainable due to steric constraints.) The orientation of the structure with respect to the membrane normal is not uniquely determined by the two angles for the 2.7 Å Mn−Mn distances. Up to eight distinct angles for the 3.3 Å Mn−Mn distance are possible. For a pair of 2.7 Å angles of 55° and 67°, these eight 3.3 Å angles are 26°, 28°, 29°, 32°, 53°, 66°, 73°, and 82°. The first four angles in the range 26°−32° correspond to an orientation with the open side of the C-shaped Mn tetranuclear cluster roughly parallel to the membrane normal (as shown in Figure 9); the second group of angles (53°−82°) corresponds to orientations with the open side of the tetranuclear structure more nearly parallel to the membrane plane. Under the assumption that the 3.3 Å EXAFS interaction is mainly determined by a Mn−Mn interaction, only the first group of angles is in agreement with the observed dichroism of the 3.3 Å EXAFS interaction (Mukerji et al., 1994; George et al., 1989). Therefore, we consider an orientation of the Mn tetranuclear complex with

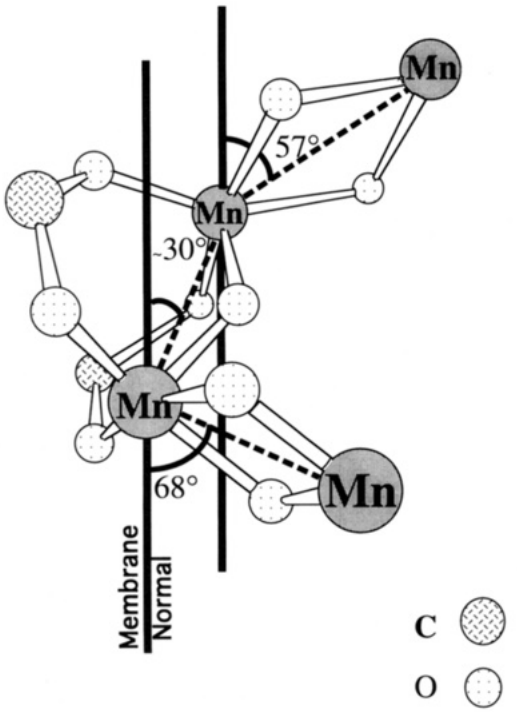

FIGURE 9: Proposed orientation of the PS II manganese complex with respect to the membrane normal. By rotation of the structure proposed by Yachandra et al. (1993) about the membrane normal, the set of angles indicated in the figure is obtainable (57° and 68°, respectively, for the 2.7 Å Mn−Mn distances; 30° for the 3.3 Å Mn−Mn distance). The rotation was done in such a way as to obtain angles for the 2.7 Å Mn−Mn distances close to the experimentally determined values of 55° and 67°, respectively. Concerning the oxidation states of the individual Mn atoms, see the Discussion.

the open side more in parallel with the membrane plane as less likely.

As indicated in Figure 9, the angle between the vector connecting the two Mn atoms of adjacent binuclear units (3.3 Å distance) and the membrane normal is predicted to be about 30°. Studies of PS II in which Sr has replaced Ca indicate that Ca probably contributes as well to the third EXAFS peak (Yachandra et al., 1993). Mukerji et al. (1994) have experimentally determined an average angle of 43° ± 10° for the vectors contributing to the third Fourier peak at 3.3 Å. However, in the study of Mukerji et al., it was not possible to discriminate between the contributions of different backscattering atoms (Mn−Mn and Mn−Ca) to the EXAFS oscillations that result in the third peak, so that even a minor contribution of a Mn−Ca interaction might result in an average angle that considerably deviates from the 3.3 Å Mn−Mn angle. Further work is in progress to resolve the dichroism of different absorber−backscatterer interactions that contribute to the third EXAFS peak of the ammonia-modified Mn complex. Comparison of the prediction of 30° for the 3.3 Å Mn−Mn vector with experimental results should be useful as a further test for the structural model proposed by Yachandra et al. (1993).

ACKNOWLEDGMENT

We thank Dr. Britton Chance for the use of his Ge detector. We are grateful to Dr. S. Khalid at NSLS and Dr. Britt Hedman at SSRL for invaluable assistance with the beam lines. H.D. thanks Dr. Horst Senger for his support and Hilmar Schiller for reading the manuscript. We thank Drs. Jean-Luc Zimmermann and Victoria J. DeRose for preliminary work with ammonia-treated PS II samples, Dr. Ishita Mukerji for providing original spectra for native oriented photosystem II samples, Dr. Annette Rompel for reading the manuscript, and Roehl Cinco for help with X-ray data collection. We thank one of the reviewers for providing valuable suggestions regarding the one- and two-shell fits to the data. Synchrotron radiation facilities were provided by the Stanford Synchrotron Radiation Laboratory and the National Synchrotron Light Source, both supported by DOE. The Biotechnology Laboratory at SSRL and beam line X9-A at NSLS are supported by the National Center for Research Resources of the National Institutes of Health.

REFERENCES

Beck, W. F., de Paula, J. C., & Brudvig, G. W. (1986) *J. Am. Chem. Soc. 108*, 4018−4022.

Berthold, D. A., Babcock, G. T., & Yocum, C. F. (1981) *FEBS Lett. 134*, 231−234.

Binsted, N., Strange, R. W., & Hasnain, S. S. (1992) *Biochemistry 31*, 12117−12125.

Blum, H., Salerno, J. C., & Leigh, J. S. (1978) *J. Magn. Reson. 30*, 385−391.

Britt, R. D., Zimmermann, J.-L., Sauer, K., & Klein, M. P. (1989) *J. Am. Chem. Soc. 111*, 3522−3532.

Brudvig, G. W., & Beck, W. F. (1992) in *Manganese Redox Enzymes* (Pecoraro, V. L., Ed.) pp 119−140, VCH Publishers, New York.

Brudvig, G. W., Casey, J. L., & Sauer, K. (1983) *Biochim. Biophys. Acta 723*, 366−371.

Bunker, G., Bunker, B. A., Crozier, D., Goulon, J., Gurman, S. J., Hasnain, S. S., Heald, S. M., Koningsberger, D. C., Natoli, R., Rehr, J. R., Sayers, D., & Udagawa, Y. (1991) *X-ray Absorption Fine Structure* (Hasnain, S. S., Ed.) p 751−770, Ellis Horwood Ltd., Chichester, U.K.

Cramer, S. P., Tench, O., Yocum, M., & George, G. N. (1988) *Nucl. Instrum. Methods A266*, 586−591.

Cristoph, G. C., Marsh, R. E., & Schaefer, W. P. (1969) *Inorg. Chem. 8*, 291−297.

Debus, R. J. (1992) *Biochim. Biophys. Acta 1102*, 269−352.

DeRose, V. J. (1990) Ph.D. Dissertation, University of California, Berkeley, CA; Lawrence Berkeley Laboratory Report LBL-30077.

DeRose, V. J., Mukerji, I., Latimer, M. J., Yachandra, V. K., Sauer, K., & Klein, M. P. (1994) *J. Am. Chem. Soc. 116*, 5239−5249.

DeRose, V. J., Latimer, M. J., Zimmermann, J.-L., Mukerji, I., Yachandra, V. K., Sauer, K., & Klein, M. P. (1995) *Chem. Phys.* (in press).

Flood, M. T., Ziolo, R. F., Early, J. E., & Gray, H. B. (1973) *Inorg. Chem. 12*, 2153−2156.

George, G. N., Prince, R. C., & Cramer, S. P. (1989) *Science 243*, 789−791.

George, G. N., Cramer, S. P., Frey, T. G., & Prince, R. C. (1993) *Biochim. Biophys. Acta 1142*, 240−252.

Goodin, D. B., Falk, K.-E., Wydrzynski, T., & Klein, M. P. (1979) in *6th Annual Stanford Synchrotron Radiation Laboratory Users Group Meeting*, SSRL Report No. 79/05, p 10−11.

Goodin, D. B., Yachandra, V. K., Britt, R. D., Sauer, K., & Klein, M. P. (1984) *Biochim. Biophys. Acta 767*, 209−216.

Guiles, R. D. (1988) Ph.D. Dissertation, University of California, Berkeley, CA; Lawrence Berkeley Laboratory Report LBL-25186.

Guiles, G. D., Yachandra, V. K., McDermott A. E., Britt, R. D., Dexheimer, S. L., Sauer, K., & Klein, M. P. (1987) in *Progress in Photosynthesis Research* (Biggins, J., Ed.) Vol. 1, pp 561−564, Martinus Nijhoff, Dordrecht, The Netherlands.

Guiles, R. D., Zimmermann, J.-L., McDermott, A. E., Yachandra, V. K., Cole, J. L., Dexheimer, S. L., Britt, R. D., Wieghardt, K., Bossek, U., Sauer, K., & Klein, M. P. (1990) *Biochemistry 29*, 471−485.

Hales, B. J., & Das Gupta, A. (1981) *Biochim. Biophys. Acta 637*, 303−311.

Heck, L., Ardon, M., Bino, A., & Zapp, J. (1988) *J. Am. Chem. Soc. 110,* 2691−2692.

Hind, G., & Whittingham, C. P. (1963) *Biochim. Biophys. Acta 75,* 194−202.

Izawa, S., Heath, R. L., & Hind, G. (1969) *Biochim. Biophys. Acta 180,* 388−398.

Kim, D. H., Britt, R. D., Klein, M. P., & Sauer, K. (1992) *Biochemistry 31,* 541−547.

Kirby, J. A., Robertson, A. S., Smith, J. P., Thompson, A. C., Cooper, S. R., & Klein, M. P. (1981) *J. Am. Chem. Soc. 103,* 5529−5537.

Klein, M. P., Sauer, K., & Yachandra, V. K. (1993) *Photosynth. Res. 38,* 265−277.

Kok, B., Forbush, B., & McGloin, M. (1970) *Photochem. Photobiol. 11,* 457−475.

Koningsberger, D. C., & Prins, R., Eds. (1988) *X-ray Absorption: Principles Applications, and Techniques of EXAFS, SEXAFS, and XANES,* Wiley-Interscience, New York.

Kretschmer, M., & Heck, L. Z. (1982) *Anorg. Allg. Chem. 490,* 215−229.

Kusunoki, M., Ono, T., Matsushita, T., Oyanagi, H., & Inoue, Y. (1990) *J. Biochem. (Tokyo) 108,* 560−567.

Larson, E. J., Riggs, P. J., Penner-Hahn, J. E., & Pecoraro, V. L. (1992) *J. Chem. Soc., Chem. Commun.,* 102−103.

Liang, W., Latimer, M. J., Dau, H., Roelofs, T. A., Yachandra, V. K., Sauer, K., & Klein, M. P. (1994) *Biochemistry 33,* 4923−4932.

MacLachlan, D. J., Hallahan, B. J., Ruffle, S. V., Nugent, J. H. A., Evans, M. C. W., Strange, R. W., & Hasnain, S. S. (1992) *Biochem. J. 285,* 569−576.

MacLachlan, D. J., Nugent, J. H. A., & Evans, M. C. W. (1994) *Biochim. Biophys. Acta 1185,* 103−111.

McKale, A. G., Veal, B. W., Paulikas, A. P., Chan, S.-K., & Knapp, G. S. (1988) *J. Am. Chem. Soc. 110,* 3763−3768.

Mukerji, I., Andrews, J. C., DeRose, V. J., Latimer, M., Yachandra, V. K., Sauer, K., & Klein, M. P. (1994) *Biochemistry 33,* 9712−9721.

Penner-Hahn, J. E., Fronko, R. M., Pecoraro, V. L., Yocum, C. F., Betts, S. D., & Bowlby, N. R. (1990) *J. Am. Chem. Soc. 112,* 2549−2557.

Riggs, R. J., Mei, R., Yocum, C. F., & Penner-Hahn, J. E. (1993) *Jpn. J. Appl. Phys., Part 1 32,* 527−529.

Rutherford, A. W. (1985) *Biochim. Biophys. Acta 807,* 189−201.

Rutherford, A. W., Zimmermann, J.-L., & Boussac, A. (1992) in *The Photosystems: Structure, Function, and Molecular Biology* (Barber, J., Ed.) pp 179−229, Elsevier, Amsterdam.

Sandusky, P. O., & Yocum, C. F. (1984) *Biochim. Biophys. Acta 766,* 603−611.

Sandusky, P. O., & Yocum, C. F. (1986) *Biochim. Biophys. Acta 849,* 85−93.

Sauer, K., Guiles, R. D., McDermott, A. E., Cole, J. L., Yachandra, V. K., Zimmermann, J.-L., Klein, M. P., Dexheimer, S. L., & Britt, R. D. (1988) *Chem. Scr. 28A,* 87−91.

Sauer, K., Yachandra, V. K., Britt, R. D., & Klein, M. P.(1992) in *Manganese Redox Enzymes* (Pecoraro, V. L., Ed.) pp 141−175, VCH Publishers, New York.

Shulman, R. G., Yafet, Y., Eisenberger, P., & Blumberg, W. E. (1976) *Proc. Natl. Acad. Sci. U.S.A. 73,* 1384−1388.

Teo, B. K. (1986) *EXAFS: Basic Principles and Data Analysis,* Springer, Berlin.

Velthuys, B. R. (1975) *Biochim. Biophys. Acta 396,* 392−401.

Wieghardt, K. (1989) *Angew. Chem., Int. Ed. Engl. 28,* 1153−1172.

Wieghardt, K. (1994) *Angew. Chem., Int. Ed. Engl. 33,* 725−728.

Yachandra, V. K., Guiles, R. D., McDermott, A., Britt, R. D., Dexheimer, S. L., Sauer, K., & Klein, M. P. (1986) *Biochim. Biophys. Acta 850,* 324−332.

Yachandra, V. K., Guiles, R. D., McDermott, A. E., Cole, J. L., Britt, R. D., Dexheimer, S. L., Sauer, K., & Klein, M. P. (1987) *Biochemistry 26,* 5974−5981.

Yachandra, V. K., DeRose, V. J., Latimer, M. J., Mukerji, I., Sauer, K., & Klein, M. P. (1992) in *Research in Photosynthesis* (Murata, N., Ed.) Vol. II, pp 281−287, Kluwer Academic Publishers, Dordrecht, The Netherlands.

Yachandra, V. K., DeRose, V. J., Latimer, M. J., Mukerji, I., Sauer, K., & Klein, M. P. (1993) *Science 260,* 675−679.

BI941422M